



This is the peer reviewed version of the following article:

Sieste, S., Mack, T., Synatschke, C. V., Schilling, C., Meyer zu Reckendorf, C., Pendi, L., et al. (2018). Water-Dispersible Polydopamine-Coated Nanofibers for Stimulation of Neuronal Growth and Adhesion. *Advanced Healthcare Materials*, 7(11): 1701485. doi:10.1002/adhm.201701485.

, which has been published in final form at: doi:10.1002/adhm.201701485.

## Water-Dispersible Polydopamine-Coated Nanofibers for Stimulation of Neuronal Growth and Adhesion

Sieste, S., Mack, T., Synatschke, C. V., Schilling, C., Meyer zu  
Reckendorf, C., Pendi, L., et al.

Article type: Full Paper

## Water-Dispersible Polydopamine-Coated Nanofibers for Stimulation of Neuronal Growth and Adhesion

*Stefanie Sieste,<sup>a,c</sup> Thomas Mack,<sup>a,c</sup> Christopher V. Synatschke,<sup>c</sup> Corinna Schilling,<sup>b</sup> Christopher Meyer zu Reckendorf,<sup>b</sup> Laura Pendi,<sup>a</sup> Sean Harvey,<sup>a,c</sup> Francesco Simone Ruggeri,<sup>d</sup> Tuomas P. J. Knowles,<sup>d</sup> Christoph Meier,<sup>a</sup> David Y. W. Ng,<sup>a,c</sup> Tanja Weil,<sup>a,c,\*</sup> Bernd Knöll<sup>b,\*</sup>*

<sup>a</sup> Institute of Organic Chemistry III/Macromolecular Chemistry,  
Ulm University,  
Albert-Einstein-Allee 11,  
89081 Ulm,  
Germany

<sup>b</sup> Institute of Physiological Chemistry,  
Ulm University,  
Albert-Einstein-Allee 11,  
89081 Ulm,  
Germany

<sup>c</sup> Department Synthesis of Macromolecules,  
Max Planck Institute for Polymer Research,  
Mainz,  
Ackermannweg 10,  
55128 Mainz,  
Germany

<sup>d</sup> Department of Chemistry,  
University of Cambridge,  
Cambridge,  
Lensfield Road,  
CB2 1EW Cambridge,  
United Kingdom

\* Correspondence should be addressed to  
Prof. Dr. Bernd Knöll (bernd.knoell@uni-ulm.de)  
or Prof. Dr. Tanja Weil (weil@mpip-mainz.mpg.de)

**Abstract**

Hybrid nanomaterials have shown great potential in regenerative medicine due to the unique opportunities to customize materials properties for effectively controlling cellular growth. We demonstrate the peptide nanofiber-mediated auto-oxidative polymerization of dopamine, resulting in stable aqueous dispersions of polydopamine-coated peptide hybrid nanofibers. The catechol residues of the polydopamine coating on the hybrid nanofibers are accessible and provide a platform for introducing functionalities in a pH-responsive polymer analogous reaction, which is demonstrated using a boronic acid modified fluorophore. The resulting hybrid nanofibers exhibit attractive properties in their cellular interactions: they enhance neuronal cell adhesion, nerve fiber growth and growth cone area, thus providing great potential in regenerative medicine. Furthermore, the facile modification by pH-responsive supramolecular polymer analog reactions allows tailoring the functional properties of the hybrid nanofibers in a reversible fashion.

**Keywords:** peptide nanofibers, amyloid fibers, polydopamine coating, neuronal growth, hybrid nanomaterial

## 1. Introduction

Amyloid fibers, formed from the self-assembly of oligopeptides into highly stable intermolecular beta-sheet structures, have conventionally been negatively associated ever since they were implicated to be the causative agent for the neuronal plaques found in Parkinson's and Alzheimer's diseases.<sup>[1]</sup> However, it has been recently shown that these fibers also serve a functional role in many native biological processes (i.e. melanin synthesis<sup>[2]</sup> and peptide hormone storage<sup>[3]</sup>) and that those neurodegenerative disease implications have rather become a question of upstream mechanisms that trigger erratically. While Nature uses amyloid fibers as a synthetic template or as efficient storage modules, chemists have exploited the excellent strength and stability to create a broad spectrum of nanomaterials<sup>[4]</sup> ranging from nanowires for optoelectronic devices<sup>[5]</sup> to hydrogel matrices<sup>[6]</sup>, drug transporters for biomedical applications<sup>[7]</sup> or as synthetic biomaterials mimicking the extracellular matrix.<sup>[8]</sup> Recently, detailed and comprehensive studies have also shown beneficial effects of bioactive amyloid fibers on neuronal cell attachment, proliferation, or neurite outgrowth.<sup>[9]</sup>

While a large number of studies have established amyloid fibers as an excellent scaffold material, the implementation of synthetic chemistry to alter the innate functionality and interactions of such fibers with cells by retaining their unique bioactivities have been much less investigated. Conceptually, by providing a very thin surface coating in a single chemical step that retains bioactivity of the amyloid fibers but also introduces functionalities for facile and reversible functionalization, one could envision a fundamental understanding of amyloid biochemistry as well as expand the range of bioapplications. Such a strategy has been recently suggested by Maji's group by applying biotechnological methods.<sup>[10]</sup> Here, peptide fragments derived from the amyloidogenic and infectious  $\alpha$ -Synuclein protein interestingly revealed biocompatibility and even promoted the differentiation of stem cells. In this regard, chemical modification techniques would provide many advantages over e.g. biotechnological methods due to the variety of functionalities that could be incorporated into the scaffold to increase the versatility of such a self-assembling platform.

Inspired by Nature's synthesis of melanin,<sup>[11]</sup> an insoluble polymer, whose polymerization is catalyzed by amyloid fibers, we hypothesize that an increase in versatility can be achieved by modifying the surface of peptide nanostructures through the facile polymerization of dopamine (DA) onto the surface of the amyloid fiber thus imparting higher degree of chemical functions. We have recently demonstrated the spatially controlled formation of polydopamine (pDA) on nanoscopic DNA origami templates using a localized redox catalyst on the nanostructure and the formation of distinct DNA origami structures due to the pDA self-adhesion.<sup>[12]</sup> pDA is a versatile biomaterial and has earned great acclaim as a multifunctional coating with applications ranging from energy, environmental to biomedical sciences due to its simplicity in formation and ability to adhere to virtually any surface.<sup>[13]</sup> Although the exact molecular structure of pDA is still under investigation,<sup>[13b, 14]</sup> the type of chemical functional groups that are present within the polymer are well known. Hence, the aforementioned applications can be achieved by using reactive groups such as amines/thiols (Schiff-base, conjugate addition) as well as the metal binding and pH-responsive capabilities of the catechols with boronic acids.<sup>[15]</sup> In combination with the mechanical and physical properties of the tightly crosslinked structure, a variety of hybrid materials that extend beyond individual components i.e. vascular devices and stents have been developed recently.<sup>[16]</sup>

Herein, we report the synthesis of hybrid peptide-polydopamine nanofibers (pDA-PNFs) that combine the nanofibrous morphology derived from PNFs (peptide nanofibers) with the versatile chemical function of pDA coatings. In this aspect, the PNFs serve both as a bioactive scaffold which promotes adhesion and growth of primary mouse neurons as well as a pre-organized template for DA polymerization on the fiber surface. Furthermore, taking advantage of pDA as a very thin, functional biocoating, we demonstrate that bioactivity of the fibrils is retained even after coating and that the catechol groups presented on the hybrid fiber surface facilitate pH-responsive and pDA-selective conjugation of cargo molecules to showcase the potential for chemical modifications of the developed platform. Next to PNFs, also pDA is known to facilitate neuronal adhesion<sup>[17]</sup> and allows for neural cell growth and proliferation,<sup>[18]</sup> and we anticipate the pDA-coating to be well tolerated by neural

cells. Hence, we envision that the fusion of amyloid and synthetic superstructures enables a multifunctional platform that allows customizing physiological and chemical properties of PNFs for regenerative medicine applications.

## 2. Results and discussion

### 2.1. DA polymerization in the presence of PNFs

#### 2.1.1. Formation and characterization of PNFs

To study the polymerization of DA in the presence of self-assembled PNFs, we chose the 8-mer *KIKIQIII* as the nanofiber forming peptide (**Figure 1a**) which was discovered by us recently. This amphiphilic peptide consists of the basic amino acid lysine (K) alternating with isoleucine (I) and a hydrophobic C-terminus, thus providing the necessary structural features to readily form self-assembled nanofibers in aqueous solutions.<sup>[19]</sup> Glutamine (Q) in the center of the sequence is further capable of stabilizing the nano-assemblies through hydrogen bonding. *KIKIQIII* was synthesized according to standard protocols based on Fmoc-protected solid phase peptide synthesis. Purification of the crude product was conducted by reversed phase high performance liquid chromatography and confirmed by matrix-assisted laser desorption/ionization mass spectrometry (**Figures S1**).

The peptide readily forms aggregates in aqueous solution when a dimethyl sulfoxide (DMSO) stock solution is diluted into a 100 mM KCl solution. After an incubation period of 18 h to ensure complete formation of PNFs and subsequent dilution into Tris-buffer at pH 8.5, the final peptide concentration was 0.5 mM. The obtained solution exhibits a significant increase in fluorescence intensity at 610 nm upon addition of the molecular rotor dye ProteoStat®, which allows for the detection of aggregate formation in peptide and protein solutions upon excitation at 550 nm (**Figure 2a**).<sup>[20]</sup>

The morphology of the peptide aggregates was investigated by transmission electron microscopy (TEM, **Figure 1b**) as well as high resolution atomic force microscopy (AFM, **Figure S2a**). The resulting images reveal well-defined nanofibers, which exceed several micrometers in length.

Secondary structure analysis obtained by Fourier-transform infrared (FT-IR) spectroscopy of a freeze-dried sample of *KIKIQIII* PNFs reveals signals in the amide I band region between 1600-1700  $\text{cm}^{-1}$  (**Figure S2b**). Using peak analysis (2nd derivative) and fitting four Gauss curves, two peaks at 1631  $\text{cm}^{-1}$  and 1692  $\text{cm}^{-1}$  were identified, indicating the formation of an anti-parallel beta-sheet structures.<sup>[21]</sup> Furthermore, the two peaks identified at 1662  $\text{cm}^{-1}$  and 1606  $\text{cm}^{-1}$  indicate formation of intermolecular hydrogen bonding of the glutamine side chains.<sup>[22]</sup>

### 2.1.2. PNFs catalyze DA polymerization

After confirming the successful fiber formation from *KIKIQIII*, we proceeded with the preparation of pDA-PNF hybrids. In the literature, several reports for the functionalization of nanofibrous structures exist; however, these mostly describe the coating of electrospun polymers rather than self-assembled peptides.<sup>[23]</sup> Notable exceptions are the coating of fibrils from tobacco mosaic virus<sup>[24]</sup> and surface grown diphenylalanine nanowires.<sup>[25]</sup>

For the formation of pDA-PNF hybrids, the polymerization of DA occurred by auto-oxidation with oxygen from air, as previously described.<sup>[13a]</sup> In the presence of PNFs, a stable aqueous solution of brown color was obtained (**Figure 1c**) indicating pDA formation. Using absorbance spectroscopy, polymerization in the presence and absence of PNFs for 24 h revealed a significant increase in pDA formation in the presence of PNFs (**Figure 1d**). The polymerization of DA is known to proceed through several intermediates beginning with the oxidation of DA to dopamine-o-quinone and subsequent cyclization to dopaminochrome followed by further oxidative and oligomerization steps until pDA is formed. The final form of pDA consists of a complex mixture of intermediates and oligomers held together by supramolecular interactions.<sup>[14]</sup> Previous studies using absorbance spectroscopy have revealed the initial presence of dopamine-o-quinone and dopaminochrome

through their characteristic absorption at around 300 nm.<sup>[15a, 26]</sup> The reaction continues with the critical oligomerization step and formation of pDA, which absorbs at higher wavelengths,<sup>[12-13, 27]</sup> ultimately yielding a material with a broad absorbance across the UV and visible spectrum as depicted in **Figure 1d**. We speculate that the formed reactive dopaminochrome intermediate subsequently reacted to DA oligomers at the surface of the PNFs due to hydrophobic interactions, mimicking the biosynthetic pathway of eumelanin formation in mammals.<sup>[2]</sup>

Detection at 320 nm was selected to determine significant differences in DA polymerization in the presence and absence of PNFs. For more accurate sample comparisons, the absorption characteristics from the early oxidation products (e.g. dopaminochrome) and pDA were recorded. As the intermediate oligomeric DA species are transitory and after very short time become indistinguishable from pDA,<sup>[14, 27]</sup> pDA will herein be used to refer to all auto-oxidation products of DA.

To further investigate the role of the PNFs on the auto-oxidative polymerization of DA, we determined the initial rate of polymerization  $v_0$  for increasing PNF and DA concentrations. We calculated  $v_0$  from the linear regression of the time resolved absorption spectroscopy during the first 60 min of polymerization by means of absorbance measured at 320 nm (**Figure S3**). When studying the effect of PNF concentration on the polymerization kinetics, we used a fixed DA concentration of 0.08 mM to avoid precipitation, which occurred at higher concentrations. We found that  $v_0$  increases with higher PNF concentrations up to 0.3 mM (**Figure 2b**) and at this concentration, the corresponding  $v_0$  value is six-fold higher than in the absence of PNFs. Interestingly, a further increase in PNF concentration leads to a decrease of  $v_0$ , which we attribute to diffusion limitation as a result of increased solution viscosity (compare PNF hydrogel formation in **Figure S2d**). Next, we varied the DA concentration, while keeping the PNF concentration at 0.5 mM. As expected,  $v_0$  initially increases with increasing DA concentrations up to 0.13 mM (**Figure 2c**). At DA concentrations above 0.13 mM, no further increase of  $v_0$  was observed. However, a black precipitate, most likely pDA, formed in the reaction vessel. To obtain colloiddally stable pDA-PNF hybrids, a concentration of 0.08 mM DA solution was used for all further experiments.

To additionally substantiate the plausible catalytic effect of the PNFs, we polymerized 0.08 mM DA in the presence of different PNF concentrations (0.0, 0.1, 0.3, and 0.5 mM, respectively) in Tris-buffer at pH 8.5. After 5 h, the formed polymer was centrifuged, washed, dissolved in 1 M NaOH and the absorption at 320 nm was measured. We found that the amount of formed pDA increases with increasing PNF concentrations. At a PNF concentration of 0.5 mM, the total amount of pDA was increased 2.6-fold compared to the sample without PNFs (**Figure 2d**). If the initiation of polymerization was to proceed by an auto-polymerization mechanism of DA, one would expect similar amounts of pDA formed in absence and presence of PNFs. However, the occurrence of higher amounts of pDA formed in presence of PNFs clearly indicates a catalytic contribution of the PNFs to the polymerization rate.

### 2.1.3. Characterization of pDA-PNF hybrid architectures

To confirm the successful formation of pDA-PNF hybrids, we performed a detailed characterization of the obtained material. Zeta potential measurements, depicted in **Figure 2e**, showed a distinct change from positive surface charges of unmodified PNFs to almost neutral in pDA-PNF hybrids, further indicating successful surface modification with pDA.

FT-IR spectra were acquired in attenuated total reflectance (ATR) mode, for the PNFs before and after DA polymerization and compared to pure pDA to verify coating (**Figure 2f** and **Figure S4**). IR bands were assigned based on the work of Zangmeister *et al.* on pDA films<sup>[28]</sup> and reference tables.<sup>[29]</sup> Observed features of pDA at 3346  $\text{cm}^{-1}$  and 3185  $\text{cm}^{-1}$  were assigned to the N-H and O-H stretching, respectively; stretching modes of aromatic C=C bonds at 1588  $\text{cm}^{-1}$  and 1460  $\text{cm}^{-1}$ ; bending of N-H at 1552  $\text{cm}^{-1}$  and stretching of C-O bonds at 1295  $\text{cm}^{-1}$ . Amide I and II bands were assigned to peaks at 1670  $\text{cm}^{-1}$  and 1540  $\text{cm}^{-1}$  of the PNF. The spectrum of pDA-PNF exhibits signals from both PNF and pDA, indicating successful polymerization of DA in the presence of fibers.

Further spectroscopic experiments were conducted with the beta-sheet prone fluorescent dye Proteostat® to investigate whether a core-shell architecture is formed upon incubation of DA in the

presence of PNFs. The increase of fluorescence emission at 610 nm ( $\lambda_{\text{ex.}} = 550$  nm) of untreated PNF solutions indicated the accessibility of binding-pockets along the fibrillar scaffold for the benzothiazole dye Proteostat®. The same experiment was also performed with PNFs, which were incubated with DA in Tris-buffer for one day at ambient temperature. The addition of ProteoStat® promoted significantly decreased emission intensities similar to the control samples containing no PNFs (**Figure 2a**). These findings suggest that the binding pockets for ProteoStat® could be blocked by pDA after polymerization further supporting that pDA-PNF hybrid material was successfully prepared.

Microscopic techniques were employed to investigate the PNF hybrid morphology in comparison to PNFs. In TEM micrographs, the unmodified PNFs were visible as fibrous aggregates, which exhibited a minor degree of bundling (**Figure 1b** and **Figure S5a**). However, the solution obtained after DA polymerization revealed dense mats of bundled fibers, with only very few fibers being present individually (**Figure 1c** and **Figure S5b**). pDA is known to be a strong bioadhesive.<sup>[13]</sup> A coating of pDA along the PNF surface could thus explain the stronger tendency for bundling in comparison to untreated PNFs.

To further substantiate the occurrence of a pDA-coating on PNFs, detailed morphological analysis was conducted by AFM (**Figure 3a-c** and **Figure S6**). Samples were deposited on mica substrates for 1 minute, avoiding clustering and allowing characterization of individual fibrils. Statistical analysis of the cross-sectional diameter of single fibers was performed by measuring the average height along the maximum height profile of the fiber, referred to as height for simplicity (**Figure 3b**). The analysis was conducted by measuring the height of all the fibrils present in each sample per unit of area on the surface of deposition (**Figure 3a, inset**). The unmodified PNFs exhibited an average cross-sectional diameter of  $2.54 \pm 0.12$  nm. This corresponded well to the estimated length of the peptide in a beta-sheet conformation of approximately 2.7 nm (**Figure S2c**). The data furthermore revealed that pDA-PNF hybrids were characterized by increased average heights of  $2.89 \pm 0.16$  nm, consistent with pDA deposition on the PNFs. Furthermore, no spherical particles corresponding to

free pDA (**Figure S7**) polymerized in solution were visible in the AFM images indicating that the polymerization mainly proceeded on the PNF surface.<sup>[30]</sup> The difference between the average of the distributions was statistically significant ( $p < 0.001$ ). However, the PNFs did not show a narrow distribution of their height and we could observe that they occurred in several polymorphs presenting different cross-sectional diameter (AFM height, **Figure S6e-g**). This was most likely due to a hierarchical assembly process of the PNFs where a different number of protofilament units make up their cross-section. The polymorphism is reflected in the statistical distribution of the cross-sectional height, which showed several peaks indicating that PNFs were therefore grouped in different polymorphs as independent distributions according to their heights (**Figure 3c** and **Figure S6**). A similar presence of multiple peaks in the statistical distribution of the cross-sectional height occurred for the pDA-PNFs, indicating again the presence of the several polymorphs. In particular, each population of the uncoated fibrils had a smaller height than the corresponding one for the coated fibrils. The comparison and averaging of the difference in cross-sectional height between individual populations of the PNFs and pDA-PNFs leads to a more accurate determination of the increase of the PNF height and the corresponding thickness upon coating. Our results therefore suggest the presence of an ultra-thin pDA coating, which appears in the order of  $0.41 \pm 0.08$  nm. The obtained results indicate a thickness of 0.2 nm for the pDA layer, which roughly corresponds to a single layer of pDA decorating the PNFs.

## 2.2. Chemical modification of the functionalized PNF hybrid surface

In macromolecular chemistry, polymer analog reactions are widely used to obtain polymeric materials with physical and chemical properties that are not available using the corresponding monomers directly.<sup>[31]</sup> In that sense, supramolecular polymer analog reactions allow modifying and adjusting the properties of polymeric materials in a stimuli-responsive fashion. Here, the polymerization of DA on the PNFs decorated the PNF surface with catechol residues. Catechol moieties undergo a specific and pH-responsive reversible covalent reaction with boronic acids which,

for instance, enables a pH-controlled release of proteins.<sup>[32]</sup> To show that the catechol groups were accessible and could be modified in a pH-responsive polymer analog reaction, we synthesized a boronic acid modified Rhodamine dye (BA-Rho, **Figure 3d** and **Supporting Information**) as a model compound and investigated its dynamic covalent interaction with the catechol groups on the pDA-PNF surface.

The pDA-PNFs were deposited on glass by drop casting. The strong adhesiveness of the pDA coating ensured a strong adsorption of the nanofibers to the surface. The dye BA-Rho was added in a PBS buffer at pH 7.4 and incubated for 30 min. After washing with PBS buffer at pH 7.4 and pH 3.0, the fluorescence of BA-Rho was measured using fluorescence microscopy. At pH 7.4, the images featured highly fluorescent deposits on the glass surface indicating successful binding of the dye to the catechol residues of pDA (**Figure 3e**). After subsequent washing with the pH 3.0 buffer, the sample did not show any fluorescent deposits (**Figure 3e, f**), indicating that the fluorescent dye had been completely removed from the pDA-PNF surface after acid treatment. Bright field microscopy images showed remaining material on glass after treatment with the washing buffers, which we presume to be pDA-PNFs (**Figure 3e**). The washing solutions were collected and measured for rhodamine fluorescence. The pH 7.4, the washing buffer showed no fluorescence, whereas the pH 3.0, the buffer revealed high fluorescence intensity, indicating the release of the BA-Rho from the pDA-coated PNFs (**Figure 3f**). The same reaction was also conducted with untreated PNFs, which were not coated with pDA as a control. No fluorescent aggregates were detected (**Figure S8**) under the same reaction conditions indicating that the fluorescent dye was exclusively bound to pDA-modified PNFs in the proposed reversible polymer analog reaction. This finding was furthermore also quantified by evaluation of microscopy images of PNFs and pDA-PNFs (**Figure S8b**).

We have demonstrated the opportunity of introducing functional groups containing boronic acid moieties selectively to the hybrid pDA-PNF, which can be exploited in the future for introducing a variety of bioactive groups. Examples of such bioactive groups are short peptide sequences<sup>[33]</sup>, DNA aptamers, reporter molecules, or proteins<sup>[32, 34]</sup> featuring boronic acid moieties

### 2.3. pDA-PNF enhance cell attachment and neurite growth of primary mouse neurons

Both pDA coatings and surface deposited PNFs were previously tested for their suitability in neural cell growth, proliferation and adhesion before.<sup>[9, 17a, 18, 35]</sup> Based on these findings, we investigated the effect of pDA-PNF hybrid coatings on adhesion and nerve fiber growth of primary postnatal mouse cerebellar neurons (**Figure 4c, f**). As a positive control, we included coverslips coated with poly-L-lysine (pll) and the extracellular matrix component laminin (lam), an established nerve fiber growth promoting substrate (**Figure 4b, e**).<sup>[36]</sup> pDA-PNFs obtained by polymerization of 0.08 mM DA in the presence of 0.5 mM PNFs were coated onto glass coverslips. Different concentrations of the coating solution were prepared by diluting the obtained pDA-PNFs, added to the cell culture substrate and dried in air to ensure reproducible coatings. Freshly prepared mouse primary neurons were spread on the modified surfaces and cultured for 72 h. The total cell number including neuronal as well as non-neuronal cells, number of neurons and average neurite length was measured via fluorescence microscopy and automated image analysis (**Figure 4**).

Compared to pDA alone or glass without any coating (**Figure 4a, d**), the pDA-PNF hybrids show an increased total number of attached cells (**Figure 4g**) as well as increased numbers of neurons (**Figure 4h**) and neurite lengths (**Figure 4i**) in a dose dependent manner. The average neurite length is comparable to pll/lam, indicating a strong promotion of neuronal attachment and nerve fiber growth of the pDA-PNF hybrids (**Figure 4i**). The total number of all cells (including non-neuronal cells) per area is significantly increased compared to the uncoated glass coverslips and pDA controls (**Figure 4g**). Above a concentration of 10  $\mu\text{g/mL}$  peptide equivalents, no further increase in cell number was detected. The number of neurons per area increases with increasing pDA-PNF concentration, indicating a beneficial effect of the pDA-PNFs on neuronal differentiation (**Figure 4h**). The average neurite length increases with increasing pDA-PNF concentration up to a length similar to that found for the pll/lam coating (**Figure 4i**).

We observed a similar impact of PNFs before and after coating with pDA on cell adhesion (**Figure 4g**) as well as comparable activity with respect to the number of attached neurons and average neurite growth (**Figure S9**). Thus, nanofibers significantly enhance adhesion of neuronal cells as well as induced neurite growth compared to uncoated surface or surfaces coated with pDA alone.

In addition to nerve fiber growth, we tested the impact of pDA-PNFs on neuronal growth cones of hippocampal neurons (**Figure 5**). Growth cones are the motile and sensory tips of nerve fibers involved in regulation of neurite extension, growth direction and axonal regeneration.<sup>[37]</sup> These structures typically consist of finger-like filopodia, which are rich in polymerized filamentous actin.

We measured the growth cone area to analyze whether pDA-PNFs have an impact on growth cone morphology. Growth cones derived from primary mouse hippocampal neurons grown on glass coverslips with no coating (**Figure 5a, d**) or pll/lam (**Figure 5b, e**) coating had a decreased number of filopodia and total growth cone area (quantified in **Figure 5g**) compared to growth cones derived from neurons plated on pDA-PNFs (**Figure 5c, f**). This suggests a stimulatory function of pDA-PNFs on growth cone morphology. Of note, the results on pDA-PNFs (**Figure 5**) are comparable to effects achieved with BDNF (brain derived neurotrophic factor), a well-established growth factor enhancing growth cone area.<sup>[38]</sup>

Thus, our results show that the beneficial effects of PNFs were retained after pDA coating yielding bioactive pDA-PNF hybrid nanostructures with clear beneficial effects on cellular attachment, nerve fiber growth, and growth cone morphology of primary mouse neurons and thus provide attractive potential for neural tissue engineering and repair.

### 3. Conclusions

We have demonstrated that PNFs obtained from the 8-mer peptide sequence *KIKIQIII* enhance the auto-oxidative polymerization of DA, resulting in catalyzed pDA formation in the presence of PNFs. Our results from concentration dependent measurements of the initial polymerization rate and the inhibited binding of an amyloid-specific dye indicate that binding sites on the PNF surface play a significant role in the formation of pDA-PNFs that are dispersible in aqueous solutions. Most likely, pDA monolayers were formed on the PNF surface and introduced catechol moieties that are accessible and could be modified in a pH-responsive polymer analog reaction. In a proof-of-concept study, we have demonstrated the selective chemical modification of pDA-coated PNF nanostructures with a boronic acid functionalized reporter chromophore. In addition to fluorescent reporter molecules, the approach may also allow for the modulation of material-cell interaction through the dynamic display of bioactive groups on the surface of the hybrid fibers. Furthermore, the pDA-coatings did not affect the biological properties of the nanostructures most likely due to the formation of an ultra-thin pDA layer.

The water-dispersible pDA-PNF hybrids were easily coated onto substrates and provide many attractive features such as the attachment and nerve fiber growth of mouse primary cerebellar and hippocampal neurons, which were comparable to the PNF backbone. Due to the unique opportunities for functionalization, we envision further optimizing pDA-PNFs application as potent nerve growth stimulating factors in neural tissue engineering or as coatings of neural implants, for example during repair strategies in the injured nervous system.

## 4. Experimental section

### *Preparation of KIKIQIII fibers and pDA-coated PNFs*

Purified *KIKIQIII* peptide was dissolved in DMSO to yield a 10.3 mM stock solution ( $c = 10 \text{ mg/mL}$ ) which was stored at  $-20 \text{ }^\circ\text{C}$  prior to usage. To initiate fiber formation, the stock solution was diluted tenfold in 100 mM KCl. The dispersed peptide was incubated for at least 18 h to ensure complete fiber formation.

For DA coating experiments, the preformed PNFs were further diluted with 10 mM Tris buffer (pH 8.5) to the concentrations as indicated in the main text. A 5.3 mM dopamine hydrochloride stock solution in demineralized water was added to the PNFs and incubated for several hours as indicated in the main text. Aliquots were taken and supplemented with 10 vol.% 1 N HCl to stop the polymerization process in time dependent measurements.

The preformed PNFs and the DA stock solution were freshly prepared prior to all experiments. A dilution scheme also including the control samples is available in the Supporting Information (**Scheme S2**).

### *FT-IR Spectroscopy*

ATR-FT-IR spectra were recorded of lyophilized sample powders of PNF, pDA, and pDA-PNF at ambient temperature using a Bruker Tensor 27 spectrometer equipped with a diamond crystal as ATR element (PIKE Miracle™) with a spectral resolution of  $2 \text{ cm}^{-1}$ . An FTIR spectrum of PNFs was furthermore obtained of lyophilized sample which was used to form a KBr pellet. The spectrum was recorded on an IFS 113v FT-IR spectrometer (Bruker) with a spectral resolution of  $2 \text{ cm}^{-1}$ . The exact compositions for all samples are given in **Table S1**.

### *Zetasizer Measurements*

The electrophoretic mobility of pDA-PNFs, *KIKIQIII* PNFs and pDA was measured to enable comparisons of surface charge changes upon coating of the material. 50  $\mu\text{L}$  of sample solutions

(prepared according to **Table S1**) were diluted in 950  $\mu\text{L}$  of 1 mM KCl-solution. The buffer was freshly prepared and filtered (pore size 0.22  $\mu\text{m}$ , Merck) prior to the experiment. The sample dispersions were introduced into separate 1 mL disposable folded capillary cells (Zetasizer Nano series, Malvern) to avoid cross contamination between samples and their electrophoretic mobility was recorded on a Zetasizer Nano ZS (Malvern Instruments) at ambient temperature. The mobility was converted to corresponding  $\zeta$ -potential values by processing the data with the Zetasizer Nano ZS Software (V7.12). The  $\zeta$ -potential was calculated by the mean value achieved of three independent measurements à 20 runs.

#### *Transmission electron microscopy (TEM)*

TEM micrographs were taken from aliquots of PNF and pDA-PNF-hybrid samples (prepared as described in **Table S1**). 5  $\mu\text{L}$  of each sample were deposited on copper grids which were coated with a thin electron-transparent Formvar-layer and were freshly etched with oxygen plasma. After 5 min incubation time, excess sample solution was removed with filter paper and the copper grid was further incubated for 5 minutes in 2% uranyl acetate solution to enhance sample contrast. After staining, the samples were washed three times in MilliQ-water, dried in air and micrographs were taken in high vacuum with an EM 109 transmission electron microscope (Zeiss) at an acceleration voltage of 80 kV. Pictures were processed with the EM109 microscope software ImageSP V1.2.6.22.

#### *Atomic force microscopy (AFM)*

AFM measurements were conducted with aliquots of pDA, PNF and pDA-PNF samples (**Table S1**) deposited on freshly etched bare mica substrates. The preparation of the mica AFM samples was realized at ambient temperature by deposition of a 10  $\mu\text{L}$  aliquot of the fully concentrated solution for 1 minute. Then the sample was rinsed with ultrapure water and dried with a gentle flow of nitrogen.

In Amplitude Modulation AFM (AM-AFM), the tip is excited with a fixed amplitude by an external force. The tip's interaction with the sample changes its motion and causes a difference between the initial and final tip amplitude, which results in a phase shift. Such phase changes reflect the dissipated energy during sample-tip interaction. By recording the phase difference, AM-AFM phase images were created simultaneously to morphology maps. High phase changes represent a strong tip-sample interaction and strong interaction force can lead to sample deformation by the tip, while low phase change represent weak tip-sample interaction.

AFM measurements of PNF (**Figure S2a** and **Figure S6a**) and pDA-PNF sample (**Figure 3a** and **Figure S6c**) were performed in air and high-resolution images (1024x1024 pixels) were collected using an NX10 Atomic Force Microscopy (Park Systems, South Korea) in ambient conditions and in non-contact AM mode. We imaged square areas of  $3 \times 3 \mu\text{m}^2$  and  $6 \times 6 \mu\text{m}^2$ . We performed all measurements using cantilevers (PPP-NCHR, Park Systems, South Korea) with a resonance frequency of 330 kHz and a typical radius of curvature of 8 nm. In order to compare the height of different samples consistently, we established standardized experimental scanning conditions and we maintained a regime of phase change in the order of  $\approx \Delta 20^\circ$ . Raw images were flattened with the XEI software (Park System, South Korea). For consistent comparison of the samples in further statistical analysis, all images were processed with the same parameters. First, images were flattened by a plane and then line by line at a 1<sup>st</sup> regression order. Then, the maximum height profile of single fibrillar structures was traced using SPIP software (Image Metrology, Denmark). We calculated the total experimental error on the cross-sectional diameter as the sum of the standard deviation, the average roughness of the sample ( $\approx 0.05$  nm) and the electrical noise of the AFM ( $\approx 0.03$  nm). The data was analyzed and histograms were created by means of OriginPro (OriginLab) software.

The pDA sample (**Figure S7**) was examined in air in tapping mode with a Multimode-AFM NanoScope (R) IV from Digital Instruments (Veeco Instruments Inc.) using cantilevers (Bruker OLTESPA-R3) with a resonance frequency of 70 kHz cantilever (2 N/m). High-resolution images (1024x1024 pixels) were processed using Gwyddion software V.2.47.

### *Fluorescence and absorption measurements*

Fluorescence spectra were recorded on an Infinite<sup>®</sup> M1000 PRO microplate reader (Tecan). Sample solutions were prepared with pDA-PNFs, *KIKIQIII* PNFs, pDA, and solvent only (**Table S1**), respectively. 9  $\mu\text{L}$  of sample aliquots were placed in black UV Star<sup>®</sup> 384 microtiter well-plates (Greiner bio-one). A ProteoStat<sup>®</sup> solution was prepared according to manufacturers' protocol and diluted tenfold in PBS. After addition of 1  $\mu\text{L}$  of ProteoStat<sup>®</sup> solution to all samples and 10 min incubation time, the fluorescence emission was recorded at 610 nm upon excitation at 550 nm. Absorption measurements were performed on the same instrument using transparent 384 microtiter well-plates (Greiner bio-one).

### *Modification of pDA-PNFs with boronic acid dye BA-Rho*

Glass coverslips (13 mm) were placed in 24-well plates (Falcon Tissue Culture Plate, flat bottom) and 75  $\mu\text{L}$  of 10-fold diluted pDA-PNFs, pDA or PNFs (prepared according to **Table S1**) were immobilized on glass *via* drop casting. After drying overnight, 150  $\mu\text{L}$  of 4 nM BA-Rho in PBS buffer at pH 7.4 were added to each well. Glass without any deposited material served as reference. The solution was incubated for 30 min, thereafter the surface was washed three times with PBS buffer. 75  $\mu\text{L}$  of PBS solution at pH 7.4 was incubated for 10 min and the supernatant was removed and analyzed *via* fluorescence spectroscopy and microscopy. Absorbance and emission spectra were recorded on an Infinite<sup>®</sup> M1000 PRO microplate reader (Tecan) between 575 and 650 nm. The fluorescence was detected upon excitation at 565 nm. For the release of the dye, the coated glass was treated 30 min with 75  $\mu\text{L}$  of a PBS buffer at pH 3.0. The supernatant solution and the glass were analyzed likewise with fluorescence spectroscopy. Microscopy images were collected after each step for all samples with a 10x objective on a Zeiss fluorescence microscope (Axiovert 200M) with bright field and Texas Red filter settings on a AxioCam MRm camera (Zeiss). All images were recorded with 500 ms

exposure time and for comparisons all brightness and contrast settings were adjusted to the same values.

#### *Mouse primary neurons*

Mouse primary cerebellar neurons were prepared from five day old (P3-P5) C57/Bl6 wild type mice as described in the literature.<sup>[36]</sup> Hippocampal neurons were derived from P1-P3 old pups. Coverslips for the positive control were coated with 100 µg/mL poly-L-lysine for 1 h at 37 °C and thereafter with 20 µg/mL Laminin overnight at 37 °C. Coverslips (13 mm in diameter) were coated by evenly distributing 50 µl of pDA-PNFs or pDA as control (concentrations given in **Figure 4**) on the cover slip and air-dried at RT overnight under sterile conditions. Before seeding cells, all coverslips were incubated in DMEM/10%HS for 30 min at 37 °C. DMEM/10%HS was then replaced by NMEM/B27 cell culture medium (with Gentamycin at 1:2000) and  $8 \times 10^3$  primary cerebellar or hippocampal neurons plated on each cover slip. Cells were fixed after 72 h in culture for 15 minutes in 4% PFA/5% Sucrose/PBS, permeabilized for 5 minutes in 0.1% Triton-X-100/PBS and blocked for 30 minutes in 2% BSA/PBS. The primary antibody against class III  $\beta$ -tubulin (1:1000; Covance) was incubated overnight at 4 °C. The primary antibody was detected with an Alexa488 conjugated secondary antibody (1:1500; Molecular Probes). Cell nuclei were labelled with DAPI and F-actin was stained with phalloidin conjugated to TexasRed.

All experiments were in accordance with institutional regulations by the local animal ethical committee (Regierungspräsidium Tübingen, Germany).

#### *Statistical analysis*

For neuronal growth assays, entire coverslips were recorded with a 4x objective on a Keyence fluorescence microscope (BZ-X700). Quantification of numbers of attached cells, nerve fiber length and growth cone area was performed with Image-Pro Plus (Media Cybernetics; version 6.0.0260) or the NeuriteTracer plug-in of the ImageJ software.<sup>[39]</sup> The plug-in analyzes fluorescence microscopy

images of neurites and nuclei of primary neurons. Employing user-defined thresholds, the plug-in counts neuronal nuclei, and traces and measures neurite length. The average neurite length was calculated automatically as a ratio of the entire neurite length of all neurons on a coverslip and the total number of DAPI-positive cells present on the coverslip. Neurons were identified by class III  $\beta$ -tubulin immunoreactivity. Growth cones were identified by F-actin localization by ImagePro Plus software. Statistical significance was calculated using Prism6 software with 2way ANOVA multiple comparison tests with \*, \*\*, \*\*\* indicating  $p \leq 0.05$ , 0.01 and 0.001, respectively. Data is displayed as mean  $\pm$  SD. N numbers are indicated in the figure legends to **Figure 4** and **5** and at least  $\geq 3$  independent cultures were performed for each condition.

Statistical analysis of the height data obtained from AFM measurements was performed with OriginPro Software using an unpaired two samples Student's t-test; \*  $p < 0.05$ , \*\*  $p < 0.01$ , \*\*\*  $p < 0.001$ ; ( $n \leq 100$ ).

### **Supporting Information**

Supporting Information is available from the Wiley Online Library or from the author.

### **Acknowledgements**

Funding is acknowledged through the BMBF project "Selekomm" within the Biotechnologie 2020+ initiative, the Carl-Zeiss foundation (CM), the Volkswagen foundation 91965 (TW, CM, SS, LP), and the Marie Curie International Training Network ProteinConjugates (TW, TPJK). BK is supported by the DFG (Deutsche Forschungsgemeinschaft) through SFB1149, the Schram, the Paul und Marlene Hepp-Stiftung, the Gemeinnützige Hertie foundation and by a research grant from an Uni Ulm - Bundeswehrkrankenhaus Ulm research initiative (Zivil-Militärischen Verbund Regenerative Medizin). CVS gratefully acknowledges support from the Humboldt Foundation through a Feodor-Lynen Return Fellowship. TPJK and FSR thank SNF (Swiss National Foundation for Science) for the financial support (grant number P2ELP2\_162116 and P300P2\_171219).

Received: ((will be filled in by the editorial staff))

Revised: ((will be filled in by the editorial staff))

Published online: ((will be filled in by the editorial staff))

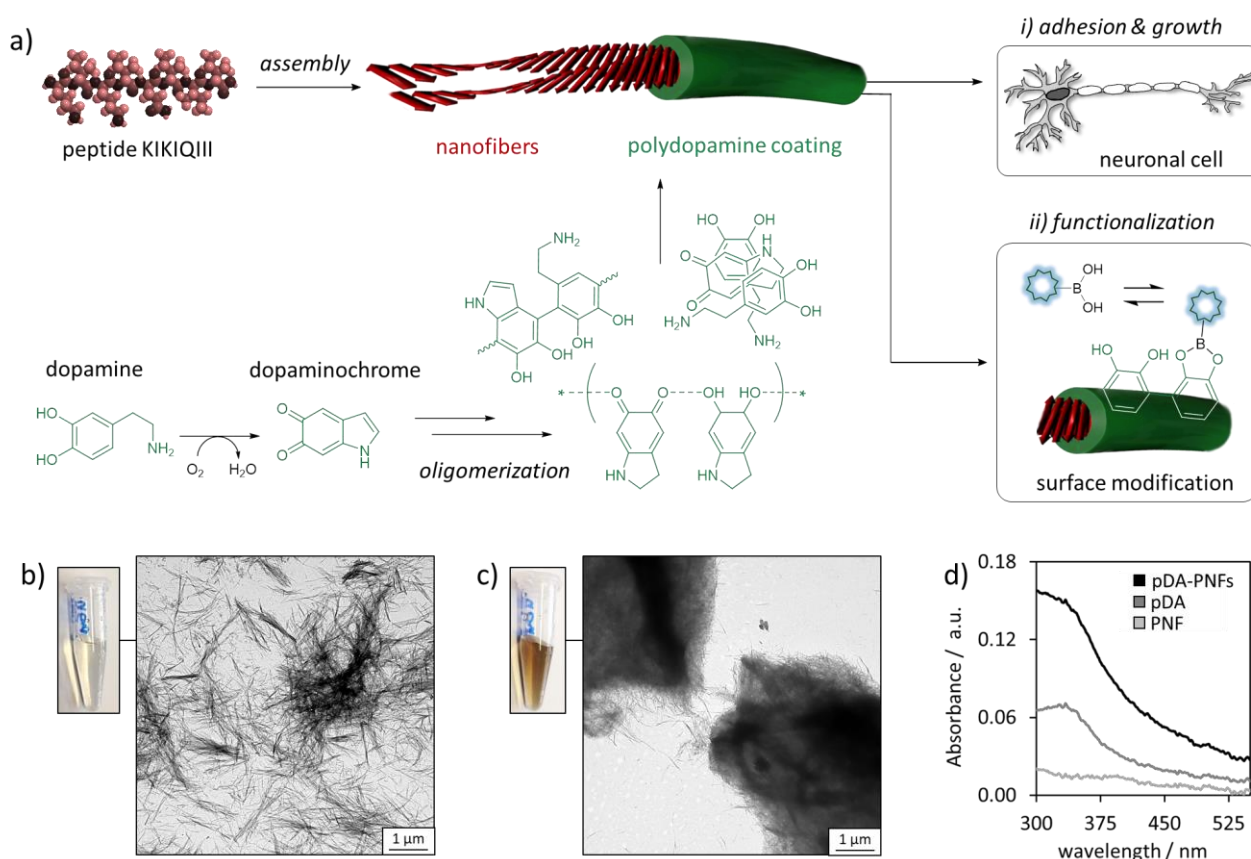


**Figure 1.** a) Schematic representation of the formation of polydopamine-coated peptide nanofiber hybrids (pDA-PNFs). Following the self-assembly of PNFs from *KIKIQIII* (red), pDA is formed on the PNF surface by auto-oxidation of DA (green). The nanostructures stimulate nerve fiber growth and the pDA-coating allows for additional functionalization. pDA intermediate structures were adapted from Tokura *et al.*<sup>[12]</sup> TEM micrographs of PNFs b) before and c) after coating with pDA. Scalebars represent 1 μm. The photographs show the respective PNF containing solutions. d) Absorption spectra of PNF, pDA, and pDA-PNF hybrid solutions. PNF and DA concentrations were 0.5 mM and 0.08 mM, respectively. pDA polymerization was carried out in Tris-buffer at pH 8.5 for 24 h at ambient temperature.

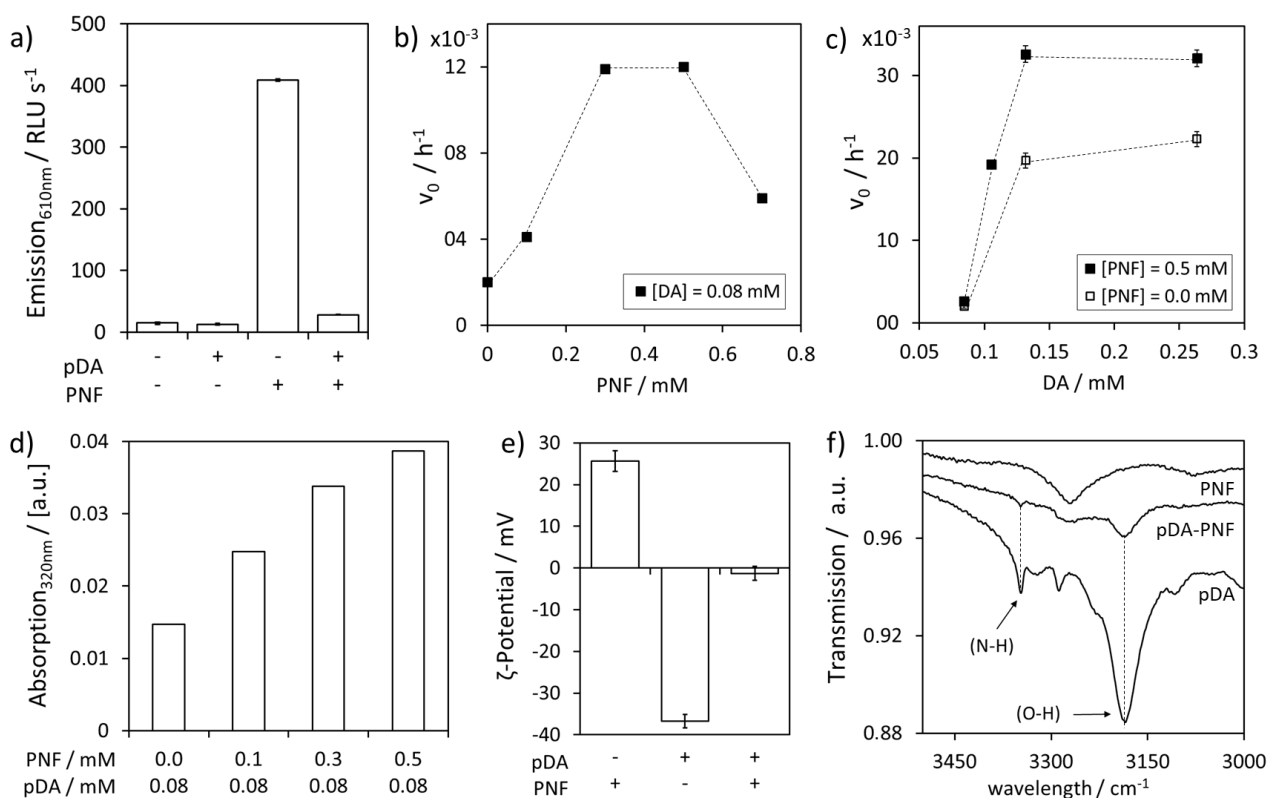


**Figure 2.** a) Increased fluorescence of the amyloid-specific dye ProteoStat® at 610 nm ( $\lambda_{\text{ex.}} = 550$  nm) upon interaction with free binding sites on PNFs. b) Initial polymerization rate  $v_0$  of DA in the presence of different amounts of *KIKIQIII* PNFs. Dopamine concentration [DA] = 0.08 mM. c) Initial polymerization rate  $v_0$  as a function of dopamine concentration [DA] in the presence or absence of PNFs. d) The absorption at 320 nm indicates the total amount of pDA formed after 5 h from 0.08 mM DA in the presence of increasing PNF concentrations. For consistent measurements, the samples were centrifuged, and the pellet was washed and dissolved in 1 M NaOH prior to the measurements. e) Zeta potential measurements of PNFs, pDA and pDA-PNF in 1 mM KCl buffer solution. f) Excerpt of FTIR spectra of lyophilized powders of PNFs, pDA and pDA-PNFs. The peaks at 3346 cm<sup>-1</sup> and 3185 cm<sup>-1</sup> are assigned to the N-H and O-H stretching bonds of pDA indicating successful polymerization in both pDA and pDA-PNF solutions. Full spectra and assignments are available in **Figure S4**. Data shown in a), e), and f) was obtained with sample concentrations as stated in **Table S1**.

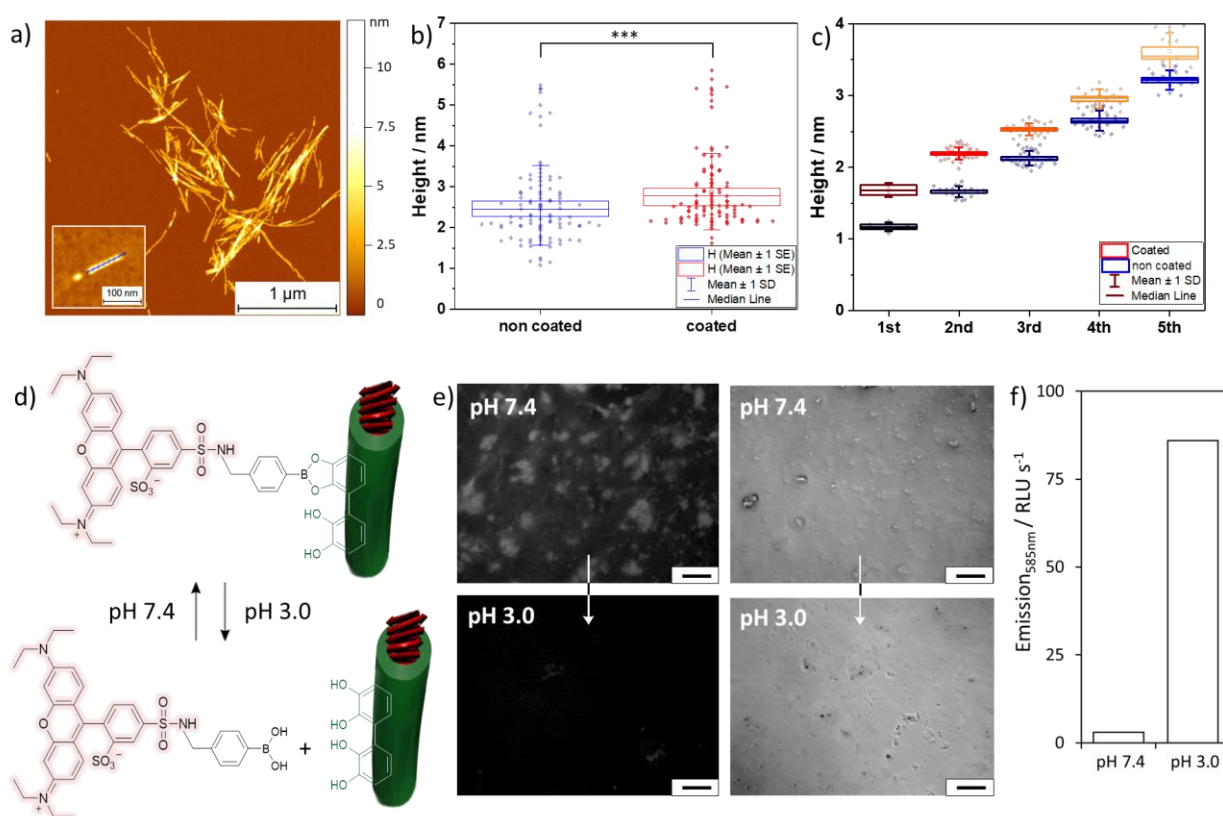


**Figure 3.** a) AFM 3-D morphology maps of PNFs after DA polymerization for 24 h using 0.5 mM PNF and 0.08 mM DA (Z scale is in nm). b) Scatter plot of the cross-sectional height of individual PNFs (n=102) and pDA-PNFs (n=100). The distributions have statistically significant differences ( $p < 0.001$ ) showing an increase in PNF diameter from  $2.54 \pm 0.12 \text{ nm}$  (blue) to  $2.89 \pm 0.16 \text{ nm}$  (red) after DA polymerization. c) The statistical distributions of height for PNF and pDA-PNFs show the occurrence of several peaks corresponding to different polymorphs of the fibrils. In particular, each PNF polymorph corresponds to a group of pDA-PNFs with increased cross-sectional diameter ( $p < 0.001$ ), enabling to measure an average coating thickness of  $0.41 \pm 0.08 \text{ nm}$ . d) Sketch of the pH-responsive modification of pDA-PNFs with fluorescent dye by reversible boronic acid-catechol interactions and e) fluorescence microscopy images of pDA-PNFs on 13 mm coverslips after incubation with boronic acid modified Rhodamine in PBS buffer at pH 7.4 and pH 3. Scalebars represent 100  $\mu\text{m}$ . f) Fluorescence emission at 585 nm ( $\lambda_{\text{ex.}} = 565 \text{ nm}$ ) of washing buffer solutions after incubation at different pH values.

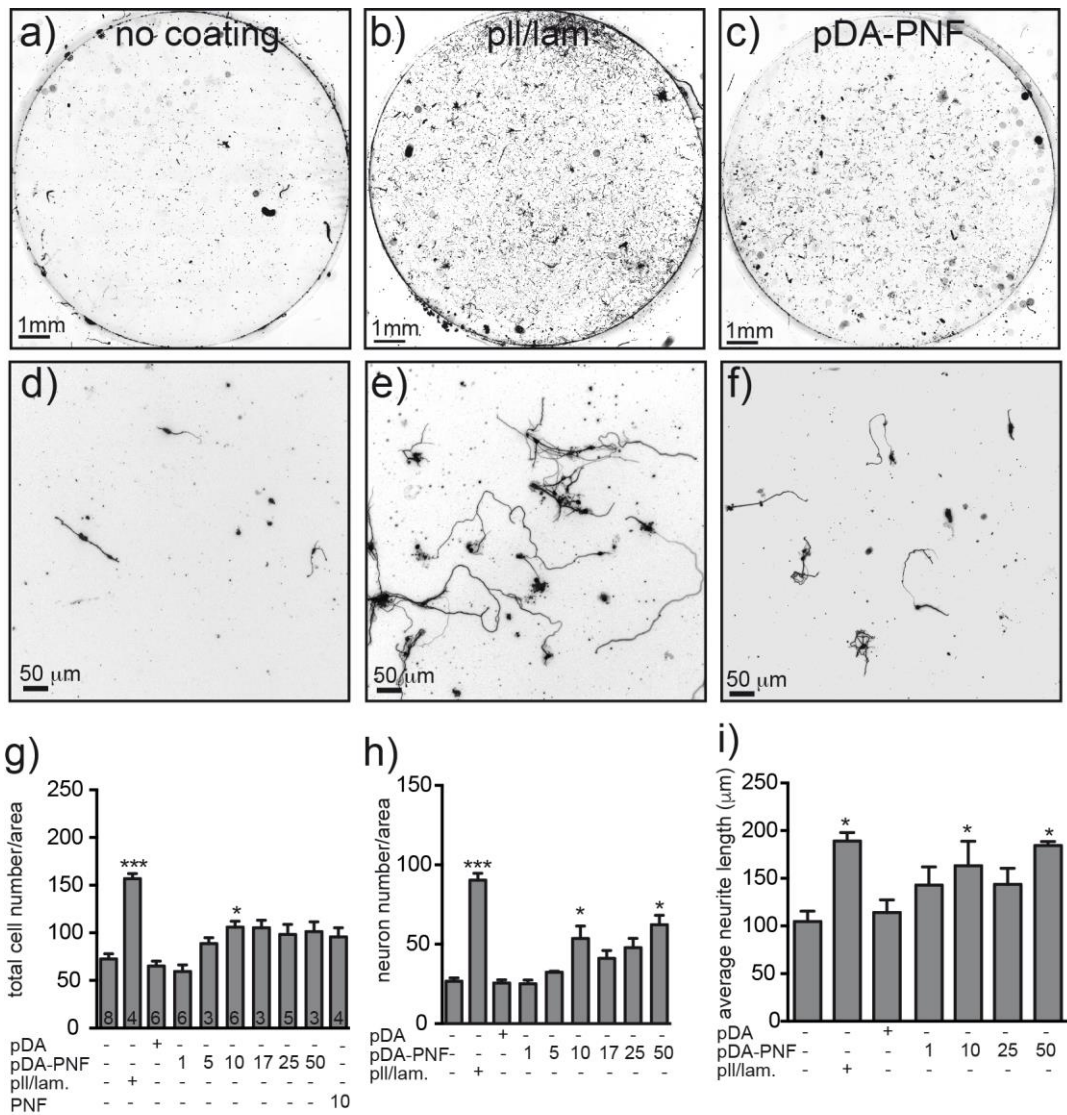


**Figure 4.** Mouse primary neuron attachment and nerve fiber growth on pDA-PNF. Neurons were cultured on unmodified glass coverslips, pll/lam coated substrates, pDA coated substrates, PNF alone or pDA-PNF coated substrates. a-c) Optical microscopy images of the entire coverslips after incubation. d-f) Magnification showing individual neuronal cells stained with the neuron-specific antibody class III  $\beta$ -tubulin. g-i) Quantification of total cell number (g), number of neurons per area (h) or average neurite length (i) obtained from the optical microscopy images. pDA concentration used for coating is 0.08 mM. pDA-PNF was obtained with 0.08 mM DA and PNF (0.5 mM peptide) and diluted to the indicated peptide concentration in  $\mu\text{g/mL}$ . \*:  $p \leq 0.05$  and \*\*\*:  $p \leq 0.001$ . 2way ANOVA was performed. N-numbers in bars (g) indicate the number of independent neuronal cultures from different mice analyzed.

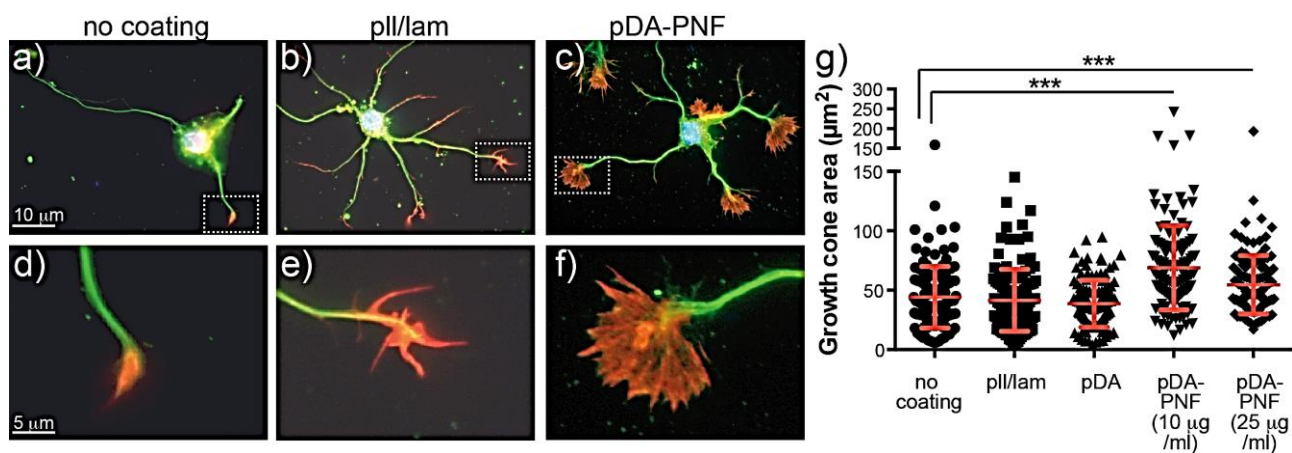


**Figure 5.** Mouse primary hippocampal neurons were plated on indicated substrates, followed by labeling for microtubules (green) and F-actin (red); the latter is used to label growth cones. Growth cone area of neurons plated on glass only (no coating; a, d) was comparable to neurons grown on coverslips coated with pll/laminin (b, e). In contrast, the growth cone area of neurons cultured on pDA-PNF was enhanced as was the number of finger-like filopodia (c, f). (d-f) are higher magnifications of dashed areas in (a-c). g) the growth cone area was quantified for the indicated conditions in at least three independent experiments. 2way ANOVA was performed. Each circle, square or triangle reflects a single growth cone. \*\*:  $p \leq 0.01$ ; \*\*\*:  $p \leq 0.001$ .

## References

- [1] D. J. Selkoe, J. Hardy, *EMBO Molecular Medicine* **2016**, 8, 595.
- [2] D. M. Fowler, A. V. Koulov, C. Alory-Jost, M. S. Marks, W. E. Balch, J. W. Kelly, *PLOS Biology* **2005**, 4, e6.
- [3] S. K. Maji, M. H. Perrin, M. R. Sawaya, S. Jessberger, K. Vadodaria, R. A. Rissman, P. S. Singru, K. P. R. Nilsson, R. Simon, D. Schubert, D. Eisenberg, J. Rivier, P. Sawchenko, W. Vale, R. Riek, *Science* **2009**, 325, 328.
- [4] a) I. W. Hamley, *Angewandte Chemie International Edition* **2007**, 46, 8128; b) G. Wei, Z. Su, N. P. Reynolds, P. Arosio, I. W. Hamley, E. Gazit, R. Mezzenga, *Chemical Society Reviews* **2017**, 46, 4661.
- [5] C. Meier, I. Lifincev, M. E. Welland, *Biomacromolecules* **2015**, 16, 558.
- [6] a) J. Boekhoven, S. I. Stupp, *Advanced Materials* **2014**, 26, 1642; b) R. S. Jacob, D. Ghosh, P. K. Singh, S. K. Basu, N. N. Jha, S. Das, P. K. Sukul, S. Patil, S. Sathaye, A. Kumar, A. Chowdhury, S. Malik, S. Sen, S. K. Maji, *Biomaterials* **2015**, 54, 97; c) G. A. Silva, C. Czeisler, K. L. Niece, E. Beniash, D. A. Harrington, J. A. Kessler, S. I. Stupp, *Science* **2004**, 303, 1352.
- [7] U. Shimanovich, I. Efimov, T. O. Mason, P. Flagmeier, A. K. Buell, A. Gedanken, S. Linse, K. S. Åkerfeldt, C. M. Dobson, D. A. Weitz, T. P. J. Knowles, *ACS Nano* **2015**, 9, 43.
- [8] R. Langer, D. A. Tirrell, *Nature* **2004**, 428, 487.
- [9] R. Pugliese, F. Gelain, *Trends in Biotechnology* **2017**, 35, 145.
- [10] S. Das, K. Zhou, D. Ghosh, N. N. Jha, P. K. Singh, R. S. Jacob, C. C. Bernard, D. I. Finkelstein, J. S. Forsythe, S. K. Maji, *NPG Asia Mater* **2016**, 8, e304.
- [11] J. M. Pawelek, A. M. Körner, *American Scientist* **1982**, 70, 136.
- [12] Y. Tokura, S. Harvey, C. Chen, Y. Wu, D. Y. W. Ng, T. Weil, *Angewandte Chemie International Edition*, DOI: 10.1002/anie.201711560n/a.
- [13] a) H. Lee, S. M. Dellatore, W. M. Miller, P. B. Messersmith, *Science* **2007**, 318, 426; b) Y. Liu, K. Ai, L. Lu, *Chemical Reviews* **2014**, 114, 5057.
- [14] a) N. F. Della Vecchia, R. Avolio, M. Alfè, M. E. Errico, A. Napolitano, M. d'Ischia, *Advanced Functional Materials* **2013**, 23, 1331; b) D. R. Dreyer, D. J. Miller, B. D. Freeman, D. R. Paul, C. W. Bielawski, *Langmuir* **2012**, 28, 6428; c) S. Hong, Y. S. Na, S. Choi, I. T. Song, W. Y. Kim, H. Lee, *Advanced Functional Materials* **2012**, 22, 4711; d) J. Liebscher, R. Mrówczyński, H. A. Scheidt, C. Filip, N. D. Hädade, R. Turcu, A. Bende, S. Beck, *Langmuir* **2013**, 29, 10539.
- [15] a) H. Lee, J. Rho, P. B. Messersmith, *Advanced Materials* **2009**, 21, 431; b) L. He, D. E. Fullenkamp, J. G. Rivera, P. B. Messersmith, *Chemical Communications* **2011**, 47, 7497; c) M. Krosgaard, V. Nue, H. Birkedal, *Chemistry – A European Journal* **2016**, 22, 844.
- [16] a) Z. Yang, Q. Tu, Y. Zhu, R. Luo, X. Li, Y. Xie, M. F. Maitz, J. Wang, N. Huang, *Advanced Healthcare Materials* **2012**, 1, 548; b) J. Sobocinski, W. Laure, M. Taha, E. Courcot, F. Chai, N. Simon, A. Addad, B. Martel, S. Haulon, P. Woisel, N. Blanchemain, J. Lyskawa, *ACS Applied Materials & Interfaces* **2014**, 6, 3575.
- [17] a) K. Kang, I. S. Choi, Y. Nam, *Biomaterials* **2011**, 32, 6374; b) K. Kang, S. Lee, R. Kim, I. S. Choi, Y. Nam, *Angewandte Chemie International Edition* **2012**, 51, 13101; c) W. C. Low, P.-O. Rujitanaroj, D.-K. Lee, P. B. Messersmith, L. W. Stanton, E. Goh, S. Y. Chew, *Biomaterials* **2013**, 34, 3581.
- [18] K. Yang, J. S. Lee, J. Kim, Y. B. Lee, H. Shin, S. H. Um, J. B. Kim, K. I. Park, H. Lee, S.-W. Cho, *Biomaterials* **2012**, 33, 6952.
- [19] N. R. Lee, C. J. Bowerman, B. L. Nilsson, *Biomacromolecules* **2013**, 14, 3267.
- [20] D. Shen, J. Coleman, E. Chan, T. P. Nicholson, L. Dai, P. W. Sheppard, W. F. Patton, *Cell Biochemistry and Biophysics* **2011**, 60, 173.

- [21] E. Cerf, R. Sarroukh, S. Tamamizu-Kato, L. Breydo, S. Derclaye, Yves F. Dufrêne, V. Narayanaswami, E. Goormaghtigh, J.-M. Ruysschaert, V. Raussens, *Biochemical Journal* **2009**, 421, 415.
- [22] A. Natalello, A. M. Frana, A. Relini, A. Apicella, G. Invernizzi, C. Casari, A. Gliozzi, S. M. Doglia, P. Tortora, M. E. Regonesi, *PLoS ONE* **2011**, 6, 1.
- [23] a) H.-j. Cho, S. K. Madhurakkat Perikamana, J.-h. Lee, J. Lee, K.-M. Lee, C. S. Shin, H. Shin, *ACS Applied Materials & Interfaces* **2014**, 6, 11225; b) J. Jiang, J. Xie, B. Ma, D. E. Bartlett, A. Xu, C. H. Wang, *Acta Biomaterialia* **2014**, 10, 1324; c) N. G. Rim, S. J. Kim, Y. M. Shin, I. Jun, D. W. Lim, J. H. Park, H. Shin, *Colloids and Surfaces B: Biointerfaces* **2012**, 91, 189; d) J. Xie, P. L. Michael, S. Zhong, B. Ma, M. R. MacEwan, C. T. Lim, *Journal of Biomedical Materials Research Part A* **2012**, 100A, 929; e) H. Yang, Y. Lan, W. Zhu, W. Li, D. Xu, J. Cui, D. Shen, G. Li, *J. Mater. Chem.* **2012**, 22, 16994.
- [24] Q. Zhou, X. Liu, Y. Tian, M. Wu, Z. Niu, *Langmuir* **2017**, 33, 9866.
- [25] J. Ryu, S. H. Ku, M. Lee, C. B. Park, *Soft Matter* **2011**, 7, 7201.
- [26] R. Liu, Y. Guo, G. Odusote, F. Qu, R. D. Priestley, *ACS Applied Materials & Interfaces* **2013**, 5, 9167.
- [27] M. Bisaglia, S. Mammi, L. Bubacco, *Journal of Biological Chemistry* **2007**, 282, 15597.
- [28] R. A. Zangmeister, T. A. Morris, M. J. Tarlov, *Langmuir* **2013**, 29, 8619.
- [29] R. Silverstein, F. Webster, D. Kiemle, *Spectrometric Identification of Organic Compounds*, John Wiley & Sons, New York **1981**.
- [30] A. Chassepot, V. Ball, *Journal of Colloid and Interface Science* **2014**, 414, 97.
- [31] K. A. Günay, P. Theato, H.-A. Klok, *Journal of Polymer Science Part A: Polymer Chemistry* **2013**, 51, 1.
- [32] D. Y. W. Ng, M. Arzt, Y. Wu, S. L. Kuan, M. Lamla, T. Weil, *Angewandte Chemie International Edition* **2014**, 53, 324.
- [33] a) J. Adams, M. Behnke, S. Chen, A. A. Cruickshank, L. R. Dick, L. Grenier, J. M. Klunder, Y.-T. Ma, L. Plamondon, R. L. Stein, *Bioorganic & Medicinal Chemistry Letters* **1998**, 8, 333; b) K. Knott, J. Fishovitz, S. B. Thorpe, I. Lee, W. L. Santos, *Organic & Biomolecular Chemistry* **2010**, 8, 3451.
- [34] C. Seidler, D. Y. W. Ng, T. Weil, *Tetrahedron* **2017**, 73, 4979.
- [35] a) C. J. Bettinger, J. P. Bruggeman, A. Misra, J. T. Borenstein, R. Langer, *Biomaterials* **2009**, 30, 3050; b) S. H. Bhang, S.-H. Kwon, S. Lee, G. C. Kim, A. M. Han, Y. H. K. Kwon, B.-S. Kim, *Biochemical and Biophysical Research Communications* **2013**, 430, 1294.
- [36] B. Knöll, O. Kretz, C. Fiedler, S. Alberti, G. Schütz, M. Frotscher, A. Nordheim, *Nature Neuroscience* **2006**, 9, 195.
- [37] F. Bradke, J. W. Fawcett, M. E. Spira, *Nature Reviews Neuroscience* **2012**, 13, 183.
- [38] C. Meier, S. Anastasiadou, B. Knöll, *PLoS ONE* **2011**, 6, 1.
- [39] M. Pool, J. Thiemann, A. Bar-Or, A. E. Fournier, *Journal of Neuroscience Methods* **2008**, 168, 134.